Science Advances
AAAS

advances.sciencemag.org/cgi/content/full/5/5/eaav7610/DC1

Supplementary Materials for

First demonstration of antimatter wave interferometry

S. Sala, A. Ariga, A. Ereditato, R. Ferragut*, M. Giammarchi*, M. Leone, C. Pistillo*, P. Scampoli

*Corresponding author. Email: rafael.ferragut@polimi.it (R.F.); marco.giammarchi@mi.infn.it (M.G.); ciro.pistillo@lhep.unibe.ch (C.P.)

Published 3 May 2019, *Sci. Adv.* **5**, eaav7610 (2019)
DOI: 10.1126/sciadv.aav7610

The PDF file includes:

Other Supplementary Material for this manuscript includes the following:

(available at advances.sciencemag.org/cgi/content/full/5/5/eaav7610/DC1)

Movie S1 (.mp4 format). Animation based on actual data from the scanned emulsion film showing the buildup of the interference pattern.

Supplementary Materials

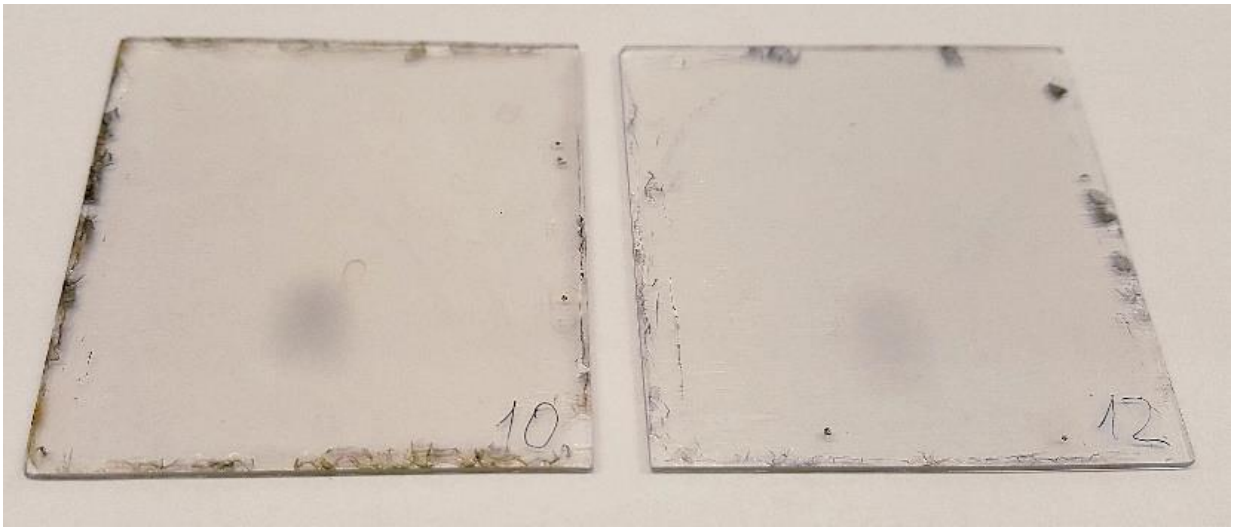

Fig. S1. **Picture of two emulsion detectors after exposure to the beam and chemical development.** (Photo credit: Ciro Pistillo, Università degli Studi di Milano).

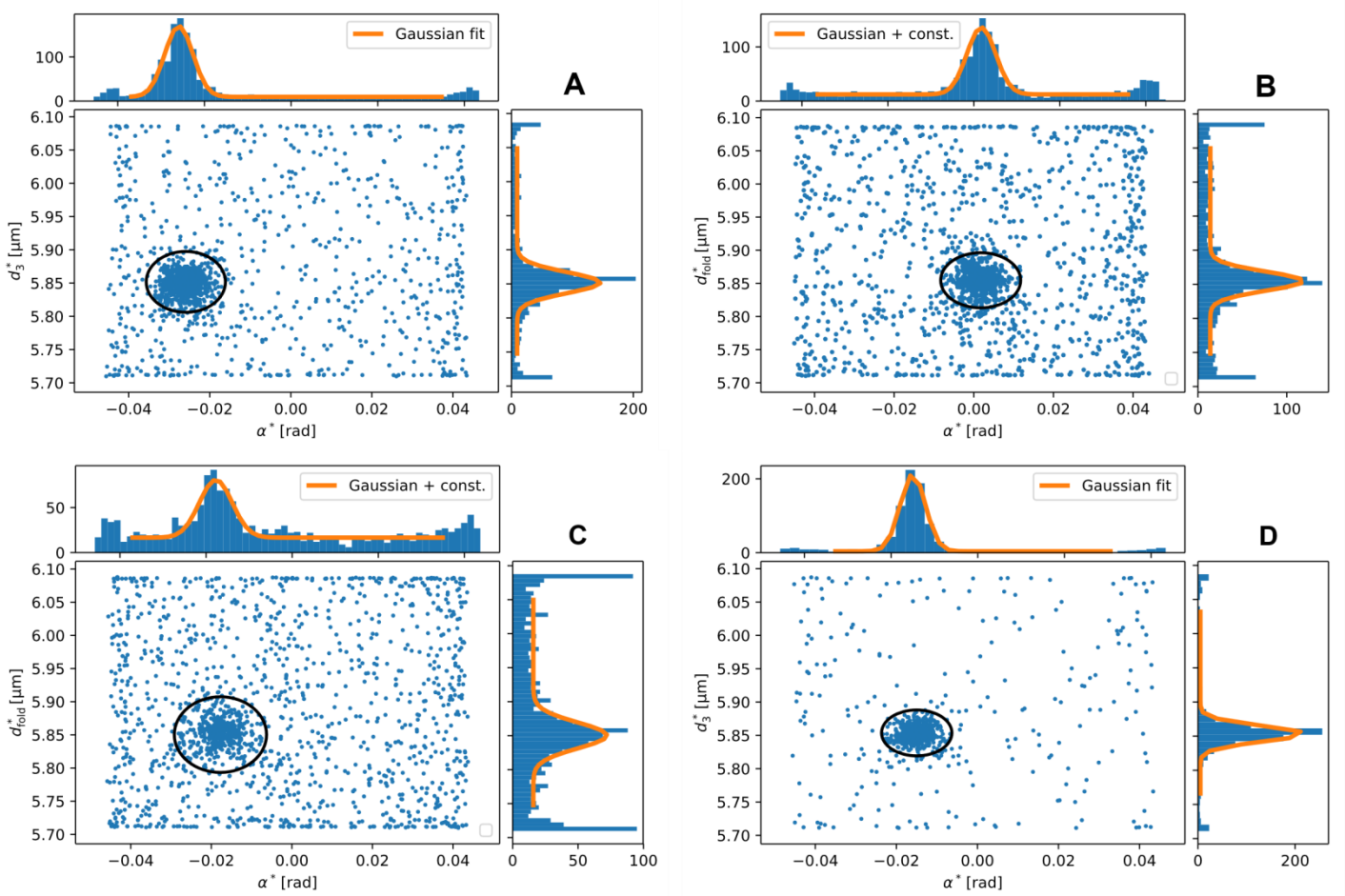

Fig. S2. Optimal angle and period found via the Rayleigh test. Results as described in Fig. 3 for positron energies of 11 keV (**A**), 9 keV (**B**), 8 keV (**C**) and 16 keV (**D**).

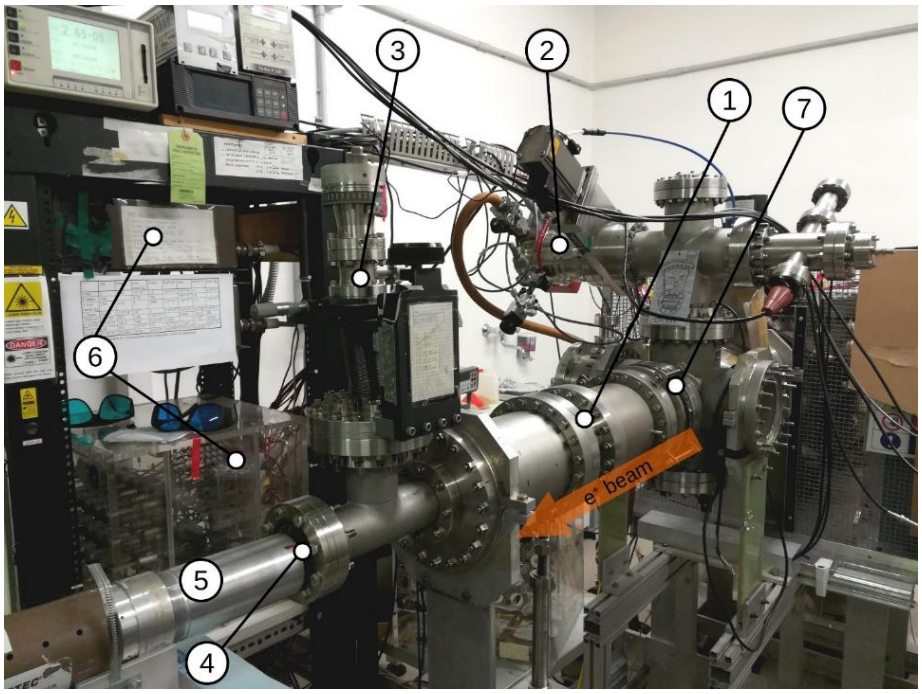

Fig. S3. Picture of the apparatus. Labelled parts are: 1) Vacuum chamber containing the interferometer and the mu-metal shield. 2) Vacuum system. 3) x-y stage moving the absorbing target for beam size measurement. 4) Viewport for laser alignment. 5) BaF_2 detector. 6) Beam control electronics. 7) Bellows used for the alignment of the interferometer chamber. (Photo credit: Simone Sala, Università degli Studi di Milano).

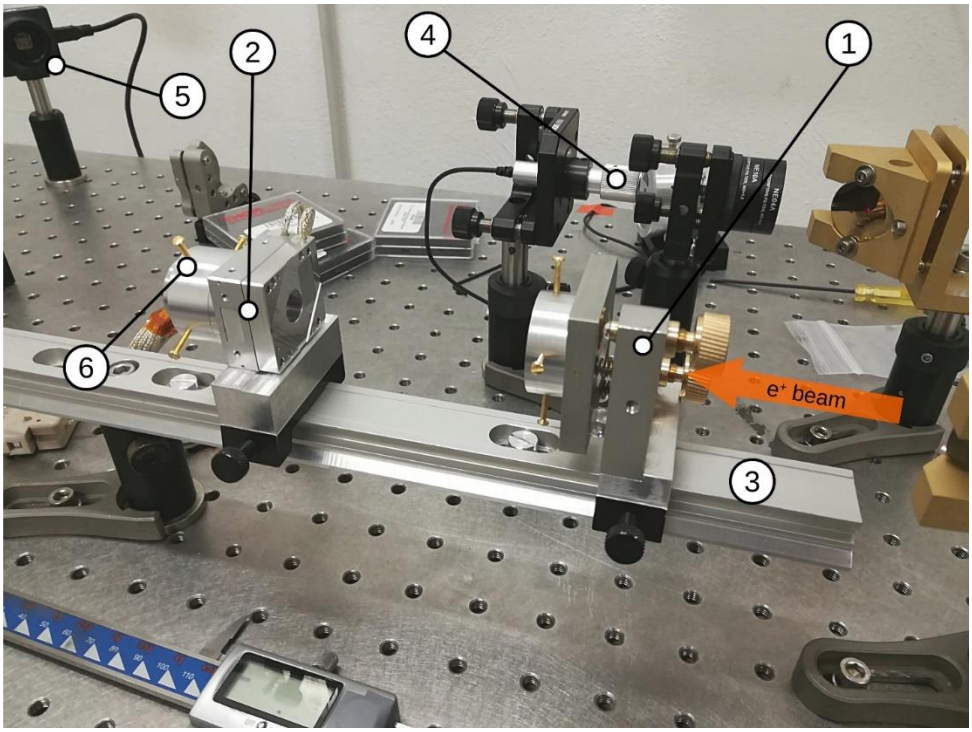

Fig. S4. Picture of the interferometer. Labelled parts are: 1) First grating mount. 2) Piezoelectric rotation stage housing the second grating. 3) Main interferometer rail. 4) Alignment laser. 5) CCD camera. 6) Grating holder with x-y adjustment screws. (Photo credit: Simone Sala, Università degli Studi di Milano).

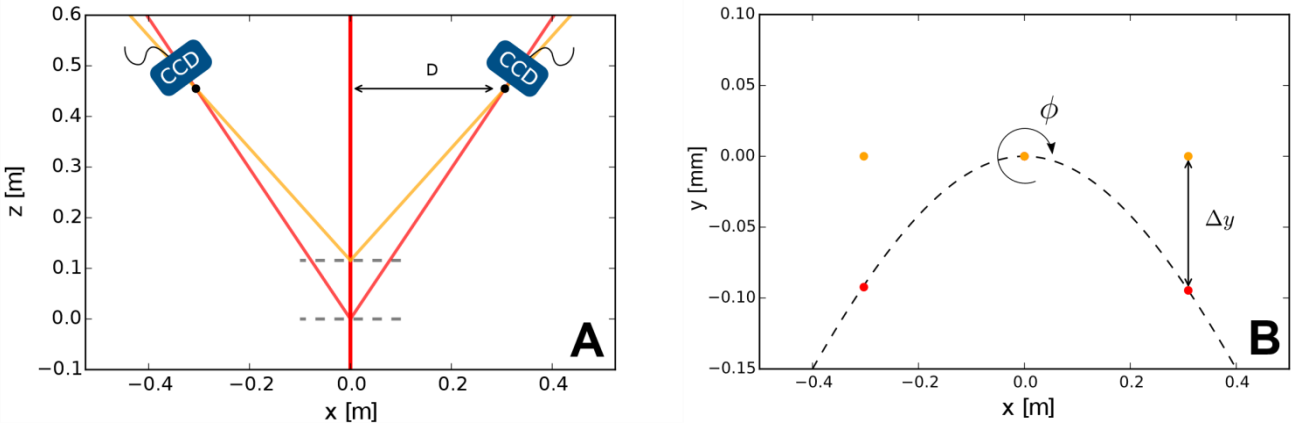

Fig. S5. Schematics of the rotational alignment procedure. A, top view of the alignment setup. The diffracted rays are indicated by the solid red and yellow lines. The dashed grey lines represent the gratings. CCD cameras are placed at the intersection points, located at a distance D ~ 0.3 m from the optical axis. **B**, position of the spots on the plane of the cameras when one of the grating is tilted about the x-axis. Spots are displaced by a distance Δy even for $\phi = 0$.

Movie S1. Animation based on actual data from the scanned emulsion film showing the buildup of the interference pattern. The data points belong to the highest contrast view at the resonance energy. From top left in clockwise order: scatter plot of the X-Y coordinates of detected positrons in the selected region of interest; folding histogram over 4 periods, to visually highlight the interference fringes; folding histogram as defined in the paper and sinusoidal fit to measure the contrast, which is displayed alongside the number of detected grains; two-parameter Rayleigh test search and maximum value. The arrival times of incoming positrons are selected randomly. This represents what a real-time detector sensitive to individual positrons would have seen during the exposure, which lasted approximately 120 hours.